Available online at www.sciencedirect.com
SCIENCE DIRECT®
International Journal of Heat and Mass Transfer 47 (2004) 539–553
International Journal of HEAT and MASS TRANSFER
www.elsevier.com/locate/ijhmt

# The role of free-surface turbulence and surfactants in air–water gas transfer

S.P. McKenna, W.R. McGillis *

*Department of Applied Ocean Physics and Engineering, Woods Hole Oceanographic Institution, Woods Hole, MA 02543-1053, USA*

Received 28 August 2001; received in revised form 30 June 2003

**Abstract**

Laboratory measurements of gas-transfer velocity and free-surface hydrodynamics were made for oscillating grid-stirred turbulence. Air–water gas-transfer velocities were determined from the waterside dissolved oxygen mass balance, and an innovative digital particle image velocimetry technique was used to measure the two-dimensional free-surface flow field. The impact of adventitious and purposely introduced surfactant films on free-surface turbulence and gas-transfer rates was explored quantitatively. As expected, bulk turbulence was unable to provide a unique relationship for the gas-transfer rates observed, owing predominantly to surfactant effects. However, the surface divergence computed from the free-surface velocity field was capable of reconciling the gas-transfer data. This is possible evidence confirming that the free-surface divergence is an important process involved in interfacial gas transport. A relationship for the gas-transfer velocity in terms of the surface divergence and the surface pressure is presented that successfully relates the interactions between surface renewal, surfactants, and gas transfer.


## 1. Introduction

The transport of gases across air–water interfaces is critically important to many fields of science and engineering. Because of this significance, a detailed understanding of air–water gas transport is desirable. Fundamentally, the exchange of gases between water and air occurs through thin boundary layers at the air–water interface where turbulent motions are suppressed giving way to molecular diffusion processes. The details of these boundary layers are determined by the aero- and hydrodynamics near the surface. For sparingly soluble gases, the airside dynamics are less critical, and the transport is determined predominantly by the waterside boundary layer [26,28]. The concentration gradient across this layer determines the flux of gas through the interface. Waterside mixing processes such as free-surface waves and near-surface turbulence act to thin this boundary layer, steepening the concentration gradient, and enhancing gas exchange.

Of key importance to air–water gas exchange are turbulent eddies near the free surface. These eddies bring fresh fluid near the interface where diffusion can take place. Increased vertical transport of fresh fluid toward the surface results in a thinner mass boundary layer. In this way, the vertical velocity fluctuations very near the interface are considered vital to gas-transfer enhancement. By continuity and using Taylor expansion, these fluctuations, $w(z)$, can be expressed as

$$w(z) = -(\nabla_h \cdot \mathbf{v})_0 z - \left[\frac{\partial}{\partial z}(\nabla_h \cdot \mathbf{v})\right]_0 \frac{z^2}{2} + \cdots \quad (1)$$

where $\nabla_h \cdot \mathbf{v}$ is the two-dimensional velocity fluctuation divergence in a plane locally tangent to the fluid interface and the subscript '0' indicates evaluation at the free surface, $z = 0$. For small $z$, higher order terms can be neglected and Eq. (1) reduces to

$$w(z) \approx -\left(\frac{\partial u}{\partial x} + \frac{\partial v}{\partial y}\right)_0 z, \quad (2)$$

* Corresponding author. Tel.: +1-508-289-3325; fax: +1-508-457-2194/2132.
*E-mail address:* wmcgillis@whoi.edu (W.R. McGillis).

0017-9310/$ - see front matter © 2003 Elsevier Ltd. All rights reserved.
doi:10.1016/j.ijheatmasstransfer.2003.06.001

**Nomenclature**

| | |
|---|---|
| $A$ | area of surface element |
| $a$ | surface divergence |
| $\mathscr{C}$ | scaling constant |
| $C_b$ | oxygen bulk concentration |
| $C_s$ | oxygen surface concentration |
| $c$ | film surface concentration |
| $D$ | molecular diffusivity of oxygen in water |
| $d$ | grid bar thickness |
| $f$ | grid oscillation frequency |
| $f_w$ | wavemaker oscillation frequency |
| $H$ | water depth |
| $\mathscr{J}$ | surface stress ratio |
| $k$ | gas-transfer velocity |
| $k^+$ | dimensionless gas-transfer velocity, $k/aL$ |
| $L$ | characteristic lengthscale |
| $L_{HT}$ | Hopfinger–Toly turbulent integral lengthscale |
| $\ell$ | turbulent integral lengthscale |
| $M$ | grid mesh size |
| $n$ | Schmidt number exponent |
| $R^2$ | regression statistic |
| $Re_a$ | Reynolds number, $aL^2/\nu$ |
| $Re_{HT}$ | empirical turbulent Reynolds number, $2u_{HT}L_{HT}/\nu$ |
| $Re_0$ | turbulent Reynolds number, $u_0\ell/\nu$ |
| $S$ | grid stroke |
| $Sc$ | Schmidt number, $\nu/D$ |
| $t$ | time |
| $u, v$ | horizontal velocity fluctuations |
| $u_{HT}$ | Hopfinger–Toly RMS horizontal turbulent velocity |
| $u_0$ | characteristic turbulent velocity scale |
| $\mathbf{v}$ | velocity fluctuation vector |
| $We_\pi$ | Weber number, $\rho u_0^2\ell/\pi$ |
| $w$ | vertical velocity fluctuations |
| $w_{HT}$ | Hopfinger–Toly RMS vertical turbulent velocity |
| $x, y$ | horizontal coordinates |
| $z$ | vertical coordinate |
| $z_s$ | distance from free surface to mean grid position |

*Greek symbols*

| | |
|---|---|
| $\alpha$ | scaling constant |
| $\delta_m$ | viscous (momentum) sublayer thickness |
| $\delta_s$ | gas (scalar) sublayer thickness |
| $\epsilon$ | static surface elastic modulus |
| $\lambda$ | scaling constant |
| $\mu$ | viscosity of water |
| $\nu$ | kinematic viscosity of water |
| $\pi$ | surface pressure |
| $\rho$ | density of water |
| $\sigma$ | surface tension |
| $\sigma_0$ | surface tension under surfactant-free conditions |

*Other symbols*

| | |
|---|---|
| $\nabla_h$ | horizontal divergence operator |
| $\bar{}$ | average |
| $\langle\ \rangle$ | temporal or ensemble average |

where $z$ is much less than the characteristic lengthscale of the horizontal velocity field near the boundary [25]. Brumley and Jirka [5] have argued that Eq. (2) is a valid approximation within one Kolmogorov scale ($\ell Re_0^{-3/4}$) of the surface, where the suppression of horizontal vorticity results in irrotational, stagnation-like flow. Expressing $w(z)$ in such a manner illustrates a direct link between gas transfer and the surface divergence: the velocity fluctuations responsible for thinning the mass boundary layer and increasing the interfacial gas flux are directly related to the divergence of the velocity field at the surface.

The hydrodynamics at a free surface are inherently complex and are made even more so due to surfactant effects [31]. Through their rheological behavior, surfactants act to damp flow at the free surface by resisting surface compression and dilation [10]. By introducing a finite interfacial stress in the plane of the interface, surfactants can create a highly dissipative viscous boundary layer where flow damping takes place. Such flow damping acts to thicken the aqueous mass boundary layer, retarding gas exchange significantly. Surfactants are often present at the air–sea interface, and are arguably present in all laboratory experiments. Therefore, careful consideration of the role surfactants play in interfacial studies is requisite.

The number of experimental efforts aimed at exploring scalar transport across air–water interfaces is seemingly endless. Some studies have focused solely on either the waterside hydrodynamics or on the airside forcing. Others have looked exclusively at the interfacial transport or the scalar concentration gradient near the interface. Some investigators have successfully examined both the flow dynamics and the transport in an attempt to develop relationships between the two. The wind-wave tunnel experiments of Komori et al. [24] in which $CO_2$ reaeration was measured along with air- and waterside velocities show promise in applying a surface renewal model to the transport process. This was accomplished by estimating the frequency of appearance

of organized motions near the interface. George et al. [13] have studied the problem of gas transfer in a vessel agitated by an array of microjets with and without a surface film. Using laser Doppler velocimetry measurements to quantify the turbulent energy levels near the interface, they show a relationship between the turbulent energy and the transfer velocity. However, the presence of a surfactant gives rise to variability in the transfer velocity for a given level of interfacial kinetic energy. Khoo and Sonin [23] have looked at a similar problem in a vessel with a single upflowing jet. Dickey et al. [12] made use of a streak photography method to quantify the waterside turbulence while simultaneously measuring gas-transfer rates for a number of gases in an oscillating grid-stirred tank. Although innovative, the results would now be considered somewhat limited as the spatial resolution of the velocity measurements was poor and measurements were not made very near the interface. Chu and Jirka [6] made concurrent measurements of near-surface profiles of turbulent velocities and $O_2$ concentration, also for grid-stirred turbulence. Likewise, Asher and Pankow [1] used a laser induced fluorescence technique to obtain bulk $CO_2$ concentration measurements for a grid-stirred system with and without a surfactant. They did not make measurements of the turbulence, but instead relied on empirical relations to characterize the flow. While these studies and many others have aided in our understanding of air–water gas transport, there are few studies in which the hydrodynamics, the transport, and the effects of surfactants are treated simultaneously. The present work utilizes new advances in particle image velocimetry (PIV) techniques to study free-surface flows with the goal of exploring relationships between air–water gas transfer, free-surface hydrodynamics, and surfactants.

## 2. Experimental approach

### 2.1. Oscillating grid-stirred turbulence

The focus of this work was to explore the relationship between interfacial turbulence and air–water mass transfer in the laboratory. Outside the laboratory, surface turbulence in lakes and the oceans is generated by several, often interrelated, mechanisms: wind-driven surface shear, waves and wave breaking, and subsurface current interactions. The turbulence generation is therefore at, or near, the water surface. Deeper sources of turbulence that manifest at water surfaces include buoyancy effects, breaking internal waves, and internal shear layers. Alternatively, in rivers and estuaries, much of the turbulence is generated from the shear at the bottom boundary. River and estuarine flows are most often simulated by open channel flumes that can be pump- or paddle-driven. Simulation of the lake and ocean environments, on the other hand, typically involves wind (-wave) flumes. A potentially significant drawback to linear, wind-wave flumes is that they are often very large and consequently impossible to maintain chemically clean. Annular wind-wave flumes, which can be much smaller and are more suitable for ''clean'' water studies, are additionally desirable because they represent closed systems. However, for both types of wave flumes, in addition to the turbulent flow, a wind-driven mean flow will exist, which can present serious complications for certain flow measurement techniques. Further complexities can arise from bottom influences, fetch dependencies, and rotational effects in annular tanks.

When studying the dynamics of an air–water interface and how these dynamics impact the flux of gases across the interface, the above facilities can prove troublesome. Complications such as physical size, contamination effects, open-loop systems, and the presence of surface waves can potentially obscure the experimental focus and make measurements prohibitively arduous. A simplified turbulence generation system is therefore desirable in such a case. In this work, the mechanism selected for the generation of turbulence was an oscillating grid-stirred tank. In such a system, turbulence is created below the air–water interface and is advected upward to the surface. Such a system might therefore be used to represent river/estuarine turbulence or subsurface-generated ocean turbulence. Grid-stirred turbulence is typically described as being zero-mean-flow, near-isotropic, and homogenous in planes parallel to the stirring grid. In addition to these experimentally favorable characteristics, a grid-stirred tank can easily be made gas-tight and of a manageable size that makes ''clean'' water experiments feasible (cf., large flumes). These features, and the fact that grid-generated turbulence has been the subject of numerous other studies (e.g., [4,11,18,34]), make such a tank a useful tool for investigating fundamental hydrodynamic processes involved in air–water mass transport. While not an ideal representation of an ocean or lake environment, the use of grid-stirred turbulence can provide the necessary groundwork for studies using more physically realistic systems.

The tank used in this study, which can be made gas-tight, has dimensions 45.4 cm × 45.4 cm × 57.2 cm deep and was constructed entirely from polycarbonate. All joints were made using a volatile chemical bond, leaving no residual solvents. Such construction avoided spurious contaminants from other types of materials and sealants. A 7×7 grid made of $d = 1.27$ cm square cross-section polycarbonate bars having a mesh size $M = 6.35$ cm was used for all experiments discussed. The grid was rigidly attached at its center point to a stainless steel shaft that passed through the tank floor with a water-tight seal provided by a stack of Teflon® V-rings. A

Table 1
Grid forcing conditions and characteristic parameters

| $S$ (cm) | $f$ (Hz) | $u_{HT}(z_s)$ (cm/s) | $Re_{HT}$ |
|---|---|---|---|
| 6.35 | 1.40 | 0.56 | 282 |
| 8.89 | 1.15 | 0.76 | 384 |
| 10.16 | 1.15 | 0.92 | 469 |
| 7.62 | 2.25 | 1.17 | 596 |
| 11.43 | 1.50 | 1.44 | 730 |
| 8.89 | 2.25 | 1.48 | 751 |
| 10.16 | 2.20 | 1.77 | 898 |
| 11.43 | 2.00 | 1.92 | 974 |

gearmotor-driven reciprocating mechanism beneath the tank vertically oscillated the shaft and grid. Using this arrangement, the water surface was completely free of obstructions. Complete details of the grid tank and the generated turbulence can be found in McKenna [29].

In all experiments, the water depth was 50.8 cm and the distance from the mean grid position to the free surface was $z_s = 25.4$ cm. Several different grid stoke, $S$, and frequency, $f$, combinations were explored. These are summarized in Table 1. Other parameters appearing in Table 1 were determined using the empirical expressions of Hopfinger and Toly [18], who found that for a planar grid of square cross-section bars with $M/d = 5$, the root-mean-square (RMS) horizontal turbulent velocity could be related to the grid parameters as

$$u_{HT} = 0.25M^{0.5}S^{1.5}fz^{-1}, \tag{3}$$

where $z$ is the vertical distance from the mean grid position. The estimated RMS vertical turbulent velocity, $w_{HT}$, was found to be 10–30% greater than the horizontal. Furthermore, the longitudinal integral length-scale was found to increase linearly with distance from the grid:

$$L_{HT} = \alpha z. \tag{4}$$

The constant $\alpha$ has been shown to fall in the range 0.1–0.4. As in Brumley and Jirka [4], our measurements indicated a choice of 0.1. The turbulent Reynolds number based on the Hopfinger and Toly values was defined as $Re_{HT} = 2u_{HT}L_{HT}/v$ and is used to characterize the bulk turbulent mixing. Note that with Eqs. (3) and (4), this Reynolds number is independent of the coordinate $z$.

### 2.2. Free-surface particle image velocimetry

PIV is a unique flow measurement technique that provides quantitative, whole-field fluid velocity information in a two-dimensional plane of interest. While PIV is becoming prevalent in experimental fluid mechanics, use of PIV at free surfaces is still novel. Gulliver and Tamburrino [16] used a quantitative imaging technique to investigate the surface flow field in a moving bed flume. A similar concept was implemented in this work using a PIV-based approach. Fig. 1 illustrates the free-surface PIV technique, and a full description of the technique can be found in McKenna [29]. An 8-bit digital CCD camera (1008 × 1018 resolution, maximum frame rate of 30 Hz) recorded the flow, which was seeded with fluorescent acrylic spheres (20–40 or 80–120 μm in diameter, specific gravity 0.92–1.1) impregnated with Rhodamine 6G and dichloro-fluorescein dyes. To remove the unwanted laser light reflection from the water surface, a precision optical bandpass filter was used. By bandpass filtering the camera, the laser light was eliminated from the images and only the PIV particles were detected. Furthermore, the details of the optical filtering and the particle fluorescence resulted in only surface particles being imaged by the camera. This eliminated concerns with the laser light cone penetrating the water column and illuminating particles at depth as well as at the surface. A more complete explanation is provided by McKenna [29], where a complementary experimental validation of the free-surface PIV technique showed that any effect of imaging particles at depth was insignificant. An advantage of the specific implementation of this surface measurement technique is the potential extension to undulating free-surface flows exhibiting small slopes and small displacements from equilibrium. This feature was exploited in this study as discussed in Section 3.3.

### 2.3. Measurement of the gas-transfer velocity

Measurements of dissolved oxygen ($O_2$) evasion were used to determine the gas-transfer velocity. Bulk water-

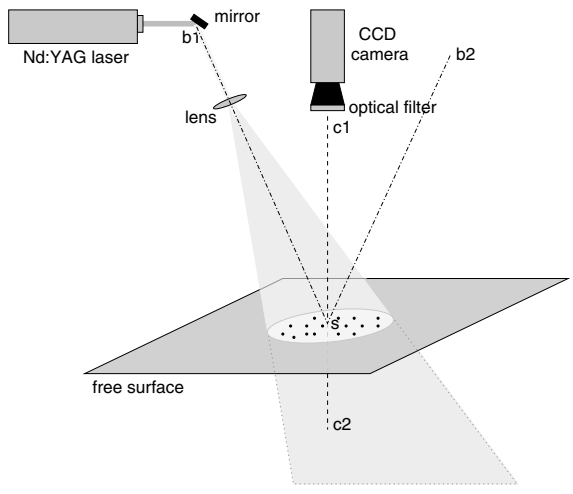


Fig. 1. PIV surface flow measurement optical arrangement. The laser beam is redirected by a high energy mirror along beam axis b1–s. A spherical lens fans the beam into a three-dimensional, diverging light cone incident on the free surface. The camera optical axis is c1–s–c2 and intersects the plane of incidence formed by b1–s–b2.

side dissolved $O_2$ concentration was measured at 0.1 Hz using a commercial water quality sensor located below the grid, 10 cm from the tank floor. Diagnostics indicated that the bulk fluid was well-mixed and the measurement of the transfer velocity was independent of sensor location. For each experiment, $N_2$ gas was used to continually flush the tank headspace to yield a known zero $O_2$ surface concentration, $C_s(t) \approx 0$ mg/l. The gas-transfer velocity $k$ was obtained using the bulk dissolved $O_2$ time-series data, $C_b(t)$, to solve the expression

$$C_b(t) = C_b(0)e^{-kt/H}, \quad (5)$$

where $H$ is the water depth and $C_s(t)$ has been taken to be zero.

## 3. Results and discussion

### 3.1. Bulk flow dynamics

Three-component fluid velocity measurements at 25 Hz using an acoustic Doppler velocimeter were used to assess the applicability of the Hopfinger–Toly (HT) relationships discussed in Section 2.1. A collection of measurements at nine different horizontal locations at an 8 cm depth indicated that Eq. (3) was an accurate model of the RMS horizontal turbulent velocity and that the RMS vertical turbulent velocity was typically 10% greater than the horizontal. A separate set of experiments using PIV in a standard light sheet mode explored the turbulent flow field in a number of two-dimensional vertical planes that spanned the tank width. Data were collected for $Re_{HT} = 596$ and 730, and provided additional evidence of the applicability of both HT relations in the bulk flow (see Fig. 2). These PIV measurements also revealed the influence of the free surface on both the turbulent velocities and the turbulent integral lengthscales. The presence of the free surface was found to slightly increase the magnitude of the near-surface RMS horizontal turbulent velocity, while reducing the RMS vertical turbulent velocity toward zero as the interface was approached. Furthermore, the horizontally measured longitudinal integral lengthscale was observed to undergo a reduction near the surface, and the horizontally measured transverse integral lengthscale was found to tend to zero at the free surface. Each of these effects was well-predicted by combined relationships using the source theory of Hunt and Graham [20] and the HT expressions [4].

### 3.2. Characteristics of the water surfaces studied

Commercially available spring water was used for the grid tank experiments. This choice was based on chemical properties and practicality considerations. Tap water was unequivocally ruled out as it is well known to contain a variety of unwanted organic material, endowing it with surface-active properties (see Fig. 3). Tap water can also show variability over the course of a day and typically shows seasonal dependence. Therefore, tap

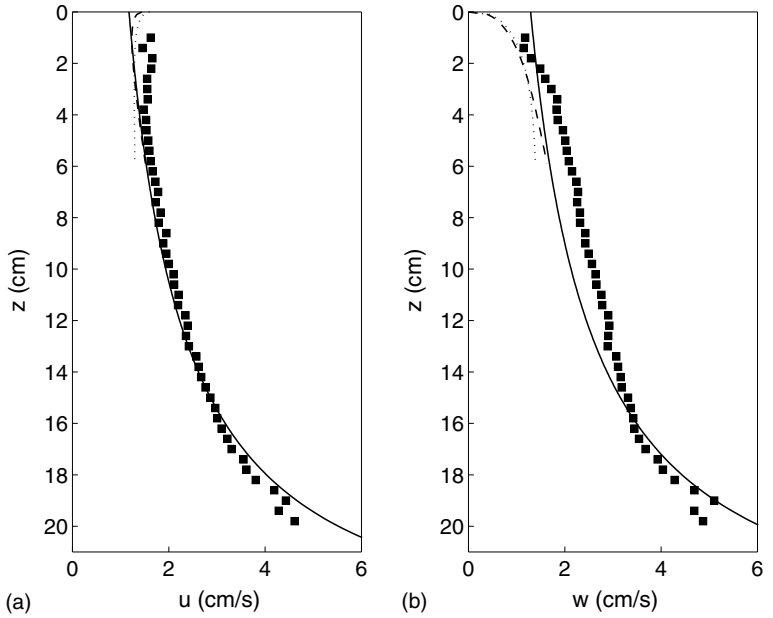


Fig. 2. Vertical profiles of spatially averaged RMS (a) horizontal and (b) vertical turbulent velocity fluctuations for $Re_{HT} = 596$. Shown are the PIV data (squares), the empirical predictions $u_{HT}$ and $w_{HT} = 1.1u_{HT}$ (solid lines), the Hunt–Graham profiles (dotted lines), and the combined profiles (dashed lines). The free surface is located at $z = 0$ and the mean grid position is at $z = 25.4$ cm.

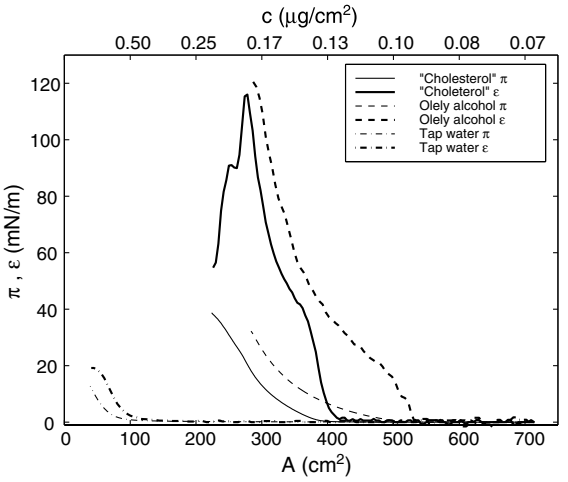


Fig. 3. Surface pressure isotherms and static surface elasticity curves for films of "cholesterol", oleyl alcohol, and tap water. For the two surfactants, spread films of 50 μg samples were analyzed. Results shown are for surfaces that were allowed to stand for 20 min. The area, $A$, corresponds to the film area. The upper abscissa reflects the film surface concentration.

water should never be used in situations where surface cleanliness is a concern. Both distilled and filtered deionized water can also contain significant levels of surface-active organics. Laboratory analysis has shown that some commercially available spring waters, while not being surfactant-free, contain very low amounts of organics and can be significantly cleaner than laboratory distilled water [14].

It is also important to realize that typical PIV seed particle mixtures can be laden with surface-active materials depending on the manufacturing process and the suspending fluid. Over the course of a number of preliminary experiments, with and without PIV measurements, it became evident that addition of a PIV seed particle mixture noticeably reduced the gas-transfer rate by roughly a factor of two. Therefore, for all the data presented here, the PIV particles used underwent a cleaning procedure that involved rinsing the PIV seed particle mixture with a 50% methanol, 50% ultra-high-pure water solution. Diagnostics indicated that this rinsing procedure was successful at eliminating the surface-active material associated with the PIV particle mixture. The addition of the rinsed particles reduced the gas-transfer velocity by only 5%.

The two surfactants used in the gas-transfer experiments were cholesterol (5α-cholesta-3β-ol) and oleyl alcohol (cis-9-octadecan-1-ol, $C_{18}H_{36}O$). Both of these surfactants are insoluble in water and form a surface film when introduced to the water surface. The choice of insoluble surfactants over soluble was made in order to focus on surface phenomena and exclude possible bulk fluid effects. Over the course of the gas-transfer work in the grid tank, the cholesterol sample showed evidence of aging in its container. As a result, the films spread using the sample cannot be considered strictly cholesterol, and therefore these results are referred to as "cholesterol," in quotes.

When a surface-active film is present at a free surface it will tend to lower the surface tension of the interface. The amount by which the surface tension is reduced is the surface pressure, $\pi$, and is defined as $\pi = \sigma_0 - \sigma$, where $\sigma_0$ is the surface tension under surfactant-free conditions and $\sigma$ is the measured tension. Fig. 3 shows adsorption isotherms for films of "cholesterol" and oleyl alcohol along with the statically derived surface elasticities for each. These $\pi$–$A$ isotherms were generated using a Langmuir–Blodgett film apparatus described in Goldman et al. [15]. The static elastic modulus is defined as $\epsilon = \mathrm{d}\sigma/\mathrm{d}\ln A$, and relates the surface stress to the dilational strain ($A$ is the area of a surface element). Under static or quasi-static conditions, a surfactant-adsorbed surface will exhibit such a surface elasticity. The surface elasticity describes the resistance of the surface to in-plane compression and dilation of the surface and is manifest in the free-surface tangential boundary condition. Under more dynamical conditions, a surfactant-adsorbed surface may exhibit rate-dependent resistance to in-plane compression and dilation, and the elastic modulus is modeled as having a viscous component. The result is a complex dynamic viscoelastic modulus. Non-zero surface (visco)elasticities modify the free-surface boundary condition and are responsible for the flow damping that causes reductions in air–water gas exchange. Results from tests with laboratory water are included in Fig. 3 to illustrate the surface-active properties of common tap water. These results can be compared with that of the spring water, which yielded maximum surface pressures of less than 0.5 mN/m and negligible surface elasticity.

### 3.3. Free-surface dynamics and air–water gas transfer

The surface PIV technique was used to quantify the free-surface flow field at four different surface locations under a variety of forcing conditions and degrees of surface cleanliness. A complete mapping of the water surface was not practical since consistent chemical surface properties could not be guaranteed over the long time period required for such a mapping. Each spatial measurement domain was roughly 6 $cm^2$ and the physical dimensions of the PIV interrogation windows were either 2.9 mm (32 px × 32 px) or 5.8 mm (64 px × 4 px) square. The majority of surface velocity data were collected in an ensemble mode with the image acquisition configured such that a pair of PIV images was collected, producing a single velocity field, every 5 s for 16 min. In this manner, spatially intensive ensemble statistics could

be computed. A second imaging technique, the time-series mode, involved a very small PIV image of the surface that yielded a $3\times3$ velocity field matrix about a single point. These images were collected continuously at 30 Hz for 10 min. Data from these sequences were used to compute time-series of turbulent velocities and derivative quantities. Concurrently, gas-transfer velocity measurements were made, yielding contemporaneous surface hydrodynamics and interfacial transport measurements. Measurements of the surface tension using the Wilhelmy plate technique [10] before and after each experimental run were used to quantify the interfacial condition in terms of the surface pressure.

The data presented represent a collection of different experiments in the grid tank. Both surface PIV and gas-transfer data were collected under a range of Reynolds numbers and for a variety of water surface conditions in order to explore the differences between a cleaned surface and surfactant surfaces for different levels of subsurface energetics. Table 2 summarizes the groups of different conditions studied. The dataset classified as 'cleaned I' refers to experiments performed in ensemble mode for an assiduously cleaned grid tank with surface aspiration occurring before individual runs. The dataset classified as 'cleaned II' was collected in the time-series mode at a single location. The 'dirty' dataset corresponds to a group of ensemble mode runs where "cholesterol" was added arbitrarily to the surface to inhibit observed surface bursting and renewal. The 'oleyl alcohol I' data correspond to two surfactant-adsorbed surfaces with the estimated surface concentrations denoted in the table. Similarly, the 'oleyl alcohol II' data reflect three surfactant-adsorbed surfaces. Both surfactant groups were studied in ensemble mode.

As a starting point, the relationship between the bulk turbulence and the gas-transfer velocity was investigated (Fig. 4). The bulk turbulence was characterized using the empirical $Re_{HT}$, which was determined to be an accurate measure of the turbulent mixing for this grid tank. Easily apparent from this figure is the inability of the bulk turbulent mixing to uniquely account for the observed transfer rates. The presence of surface-active material is seen to reduce the transfer velocity by as much as a factor of four for a given $Re_{HT}$. This is not a surprising result since air–water transport is a process that is strongly linked to the dynamics very near the free surface, which is where surfactant effects are most dominant. Bulk turbulence away from the interface is largely unaffected by surface films and therefore cannot accurately predict the levels of gas transport. Also included in Fig. 4 are the grid-stirred tank gas-transfer measurements of Chu and Jirka [6]. These measurements were obtained in a tank 50 cm square by 40 cm deep with an $8\times8$ grid having the same $M$ and $d$ as the grid used in this study. The grid was located 25 cm from the water surface and oscillated vertically. The Chu and Jirka system is therefore relatively similar to the present system. The transfer velocity for $O_2$ was estimated in a

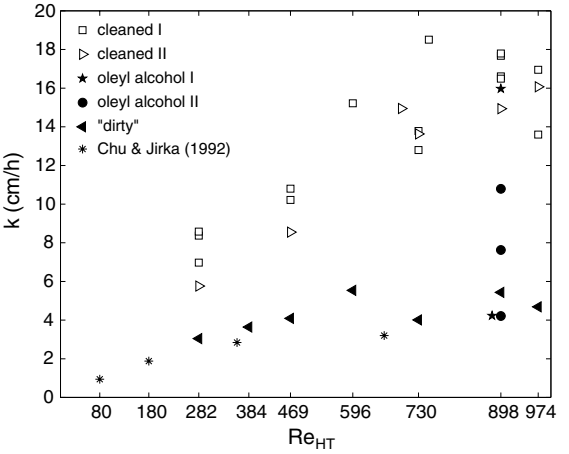


Fig. 4. Dependence of the gas-transfer velocity on bulk turbulent Reynolds number for grid-stirred turbulence. The figure key specifies the respective datasets, which are discussed in the text and Table 2.

Table 2
Summary of the surface PIV/gas-transfer experimental conditions

| Dataset name | $Re_{HT}$ included | $\bar{\pi}$[a] (mN/m) |
|---|---|---|
| Cleaned I | 282, 469, 596, 730, 751, 898, 974 | $-0.01\pm0.28$ |
| Cleaned II | 282, 469, 596, 730, 898, 974 | $-0.16\pm0.28$ |
| Dirty | 282, 384, 469, 596 | $1.16\pm0.27$ |
| | 730, 898, 974 | $3.51\pm0.26$ |
| Oleyl alcohol I[b] | 898 ($c=0.013$ μg/cm$^2$) | $0.24\pm0.27$ |
| | 898 ($c=0.138$ μg/cm$^2$) | $2.87\pm0.27$ |
| Oleyl alcohol II[b] | 898 ($c=0.043$ μg/cm$^2$) | $0.75\pm0.27$ |
| | 898 ($c=0.061$ μg/cm$^2$) | $1.12\pm0.27$ |
| | 898 ($c=0.091$ μg/cm$^2$) | $1.28\pm0.27$ |

[a] The values for surface pressure $\bar{\pi}$ reflect the average of the individual cases within each dataset.
[b] For the oleyl alcohol datasets, $c$ refers to the estimated film surface concentration.

manner similar to that used here except that the bulk $O_2$ concentration was monitored over the course of 10 h. It is apparent that over this long period of time, the average gas-transfer velocity was considerably less than that measured for the present cleaned system. It is possible that the difference can be explained by adventitious surface films present in the Chu and Jirka experiments. The authors mention cleaning the surface, but do not report a measure of the degree of cleanliness.

Shown in Fig. 5(a) are the same gas-transfer measurements plotted against a measure of the free-surface turbulent mixing, $\langle u \rangle$, which reflects the temporally or ensemble averaged surface RMS velocity fluctuations. Each $\langle u \rangle$ value derives from a measurement record that is coincident with the measurement of the gas-transfer velocity. Relating $k$ to $\langle u \rangle$ reduces some of the scatter in the data and suggests a clearer monotonic trend. The $R^2$ regression statistic for these data was 0.62. However, the relationship is still somewhat degraded by surface film

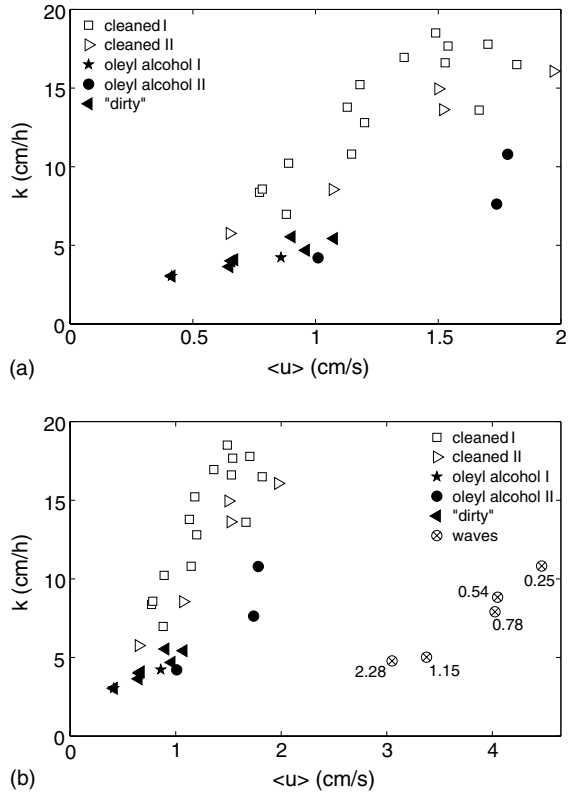


Fig. 5. Dependence of the gas-transfer velocity on surface RMS velocity fluctuations for (a) grid-stirred turbulence, $R^2 = 0.62$, and (b) grid turbulence and mechanically generated surface waves, $R^2 = 0.02$. For the waves data, values of surface pressure (in mN/m, ±0.27 mN/m) for each run are indicated next to the markers. Increasing $\pi$ corresponds directly to increasing surfactant concentration.

influences. The transfer velocities observed for cleaned conditions were consistently higher than those for surfactant conditions. Fig. 5(b) is identical to Fig. 5(a), but also includes data collected from an experiment that investigated the effects of mechanically generated waves on gas exchange (identified as 'waves'). This experiment was conducted in the grid tank and the measurement procedure for the transfer velocity was identical to that for the grid-stirred runs. Surface waves were generated using a plunger-type wavemaker positioned along one wall of the tank and spanning the width of the tank. The wavemaker was forced at a frequency of 3.2 Hz. The resulting wave field was dominated by quasi-steady, two-dimensional standing waves having amplitudes of less than 2 cm. These mechanical waves were simple to generate and provided a completely different flow type for study. In an effort to keep the grid tank reasonably well-mixed during the wave runs, the grid was oscillated in a low energy state: $S = 10.16$ cm, $f = 0.5$ Hz. Measurement of the transfer velocity under this forcing alone without waves indicated extremely small gas-transfer enhancement ($k \approx 2$ cm/h). Surface PIV measurements were made at a single location in the center region of the tank in the ensemble imaging mode. Sequential runs were performed with increasing concentrations of spread oleyl alcohol films as discussed in the figure.

Clearly, the magnitudes of the fluctuations induced by the wave field are much higher than the turbulent fluctuations created by the oscillating grid alone. Even when the surface was covered with the highest concentrations of oleyl alcohol, the fluctuations from the waves were still higher than any observed for the grid turbulence. However, the gas-transfer velocities were not found to be correspondingly greater. In the case of the waves dataset, the surface flow field was predominantly a sloshing wave mode in which significant surface velocities were generated. However, although appearing as velocity fluctuations, the wave orbital velocities are not turbulent and do not have the same effect on interfacial transport. The velocity fluctuations associated with these artificial waves are not effective in creating surface renewal and enhancing gas exchange. It appears that while the surface velocity fluctuations provide an improved relationship for the gas transfer when compared to a bulk turbulence estimate, such a parameterization is dependent upon the particular type of flow. This is reflected in the near-zero $R^2$ regression statistic for the combined datasets.

To explore the role of surface divergence, the gas-transfer data shown in Fig. 5(b) are replotted against a measure of the divergence in Fig. 6. For the data collected from the spatially intensive measurements at the four PIV locations, $\langle a \rangle$ is an ensemble-averaged value of the magnitude of the divergence. The divergence was computed from the first-order finite difference of the velocity field. In the case of the time-series data, $\langle a \rangle$ was

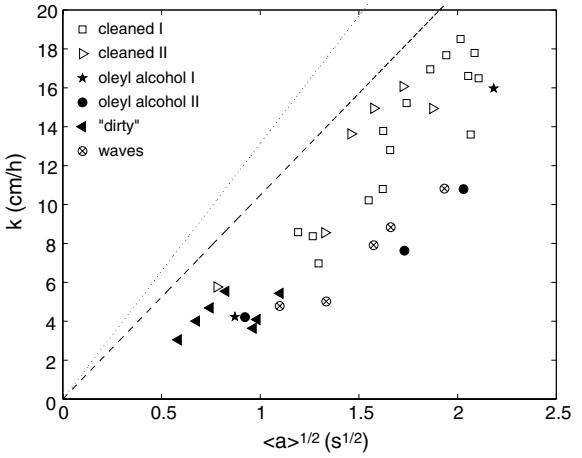


Fig. 6. Dependence of the gas-transfer velocity on surface divergence for grid-stirred turbulence and mechanically generated surface waves. The dashed line corresponds to the limiting result of Ledwell [25], $k \rightarrow (2/\pi)(Da)^{1/2}$. The dotted line corresponds to the Csanady [8] result, $k = \sqrt{2/\pi}(Da)^{1/2}$. $R^2 = 0.77$.

estimated from the integrated spectral density function for the divergence, as suggested by McCready et al. [27]. The striking feature of this figure, in addition to the favorable monotonic trend, is the fact that both flow types, grid turbulence and surface waves, are reconciled by the surface divergence. For grid turbulence alone, $R^2 = 0.82$, an improvement over the $k$–$\langle u \rangle$ relationship, and for both turbulence and waves, the result is nearly identical, $R^2 = 0.77$. Also included in this figure are the simple transfer velocity predictions of Ledwell [25] and Csanady [8]. The Ledwell prediction derives from a simple eddy diffusivity model that used scaling arguments to deduce a limiting result for a clean interface. Csanady solved the convection–diffusion equation assuming a steady, two-dimensional stagnation flow to arrive at the result shown in Fig. 6.

### 3.4. Effect of surface films on gas transfer

As already seen, the impact of a surface film on free-surface hydrodynamics is marked. The entire nature of the surface flow field is modified by the simple addition of a tangential stress in the plane of the interface. To demonstrate this effect, two velocity field realizations for $Re_{HT} = 898$ are presented. Fig. 7 shows a case from the cleaned I dataset and a case from the oleyl alcohol II dataset. The velocity field for the cleaned surface condition is dominated by numerous areas of surface bursting. These surface bursting motions are the result of turbulent eddies impinging at the surface in random fashion. The velocity field for the surfactant surface, however, appears less chaotic and is noticeably weaker. A large eddy motion is observed with other meandering

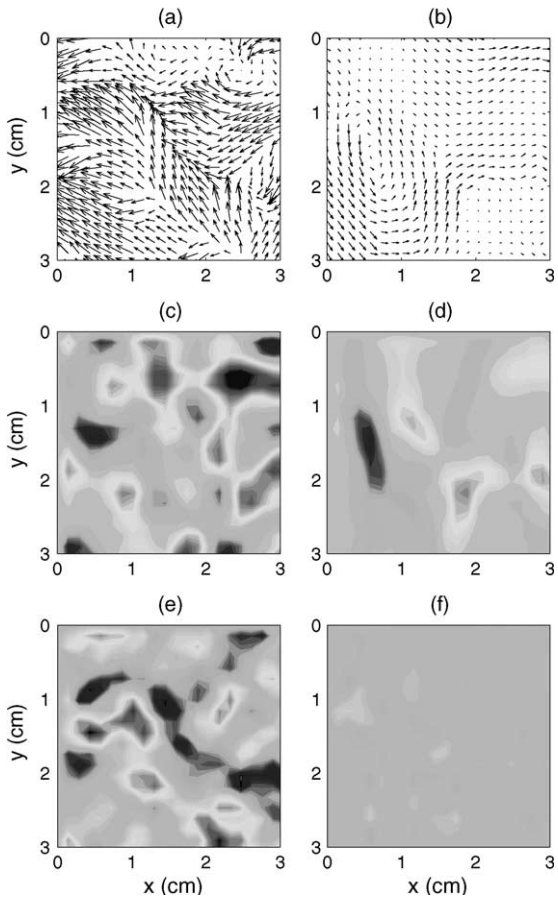


Fig. 7. Surface flow fields for cleaned and surfactant surfaces. The left panels correspond to a cleaned I run at $Re_{HT} = 898$. The right panels correspond to the oleyl alcohol II run with $c = 0.091$ μg/cm$^2$ (also at $Re_{HT} = 898$). (a,b) The velocity fields; the vectors in each panel have been scaled equally. (c,d) Contours of vorticity; the contour levels are the same for both panels: −15 to 15 s$^{-1}$ in increments of 1 s$^{-1}$. (e,f) Contours of divergence; the contour levels are the same for both panels: −15 to 20 s$^{-1}$ in increments of 1.25 s$^{-1}$.

flow structures in the vicinity. The vorticity fields are also dramatically different. In the cleaned case, the surface is populated with many local regions of both positive and negative vorticity. In the surfactant case, only two or three regions of vorticity are detectable, the most obvious being related to the large surface eddy seen in the velocity field. The comparison between the two surface divergence fields follows similarly. The cleaned case exhibits frequent areas of intense divergence, while the surfactant case shows very weak flow divergence. These two examples illustrate that under reasonably clean conditions, the free surface is highly dynamic and energetic. The surface flow field is dominated by local regions of intense vorticity and divergence. The scales associated with these shearing and straining motions are

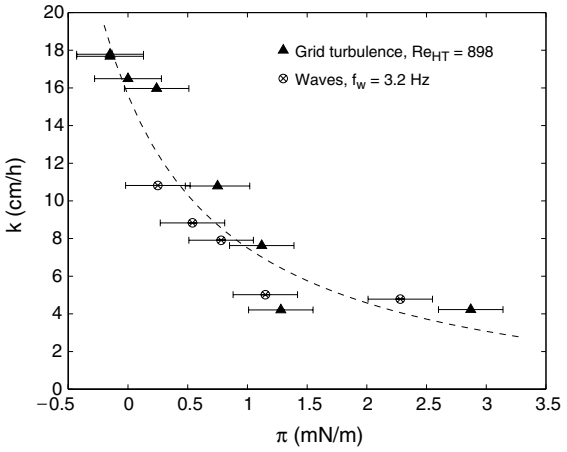


Fig. 8. Influence of surface pressure on gas-transfer velocity for grid-stirred turbulence and mechanically generated surface waves. The frequency $f_w$ corresponds to the wavemaker frequency. The horizontal bars indicate the 95% confidence intervals for the surface pressure measurements. The dashed line is an inferred $\pi^{-1}$ trend line.

relatively small, on the order of 1 cm. When a surfactant is introduced, the surface flow becomes highly damped and the entire flow field is modified. The surface turbulence is reduced, in turn reducing the intensities of the vorticity and divergence. Furthermore, the flow appears to become nearly void of strong surface renewal events and is better characterized by a mosaic of meandering weak eddy motions. It also was observed that the presence of surfactant increased the turbulent lengthscales of the flow. Similar results looking at surface temperature fields have been shown recently by Saylor et al. [30] in evaporative convection experiments with and without surfactant.

The oleyl alcohol I, II and waves datasets provide measurements of the gas-transfer velocity for varying levels of surface pressure for two different types of flow. To visualize the impact of a surface film on gas transfer, Fig. 8 shows these three datasets in a $k$–$\pi$ relationship. The fact that both the grid turbulence data for $Re_{HT} = 898$ and the wave data can appear on the same plot is coincidental. The trend seen in this figure is not unlike other trends observed for the effect of surface pressure on gas-transfer velocity [15], surface turbulence, vorticity, and divergence [29]. The greatest impact of the surfactant is realized at very small levels of surface pressure (less than about 1.5 mN/m); beyond 1.5 mN/m, the reduction in $k$ remains nearly constant.

### 3.5. The nature of turbulence near air–water interfaces

It is useful to summarize the key aspects of our current understanding of free-surface turbulence and air–water gas exchange in terms of conceptual models, simulations, theory, and observations. Conceptualizations of the effects of surface films on free-surface turbulence have been suggested by Davies [9], Davies and Rideal [10] and Hunt [19]. Laminar interactions between a surfactant surface and a subsurface vortical flow have been studied numerically by Tsai and Yue [36], and turbulent interactions near clean and surfactant surfaces have been explored similarly in terms of scalar transport by Tsai [35]. From these studies and others, an understanding of the turbulence near clean and surfactant air–water interfaces emerges that relates to the experimental observations in the present study. First, the clean case may be considered. In this case, assuming a flat surface, there are two main effects of the free surface on the turbulence below: (1) an irrotational "blocking" effect that results from the kinematic boundary condition at the free surface constraining the vertical motion at the surface, and (2) a viscous effect resulting from the dynamic boundary condition at the surface that prescribes near-zero tangential stress at the interface. The blocking effect results from the constraint that eddies are restricted from approaching the surface closer than a distance equal to their size. Therefore, the effect is related directly to the eddy lengthscales and should extend over a depth roughly equal to the integral lengthscale of the turbulence ($\ell$). For a clean interface, within this region, the consequence is a reduction in the turbulent vertical velocity fluctuations resulting in an increase in the horizontal velocity fluctuations through a redistribution of the turbulent energy. Shen et al. [32] have shown that this region also defines the depth over which the turbulent diffusivity is affected by the free surface. These effects arise from the flow adjusting to the free-surface condition that states $w = 0$ on $z = 0$, where $z = 0$ indicates the location of the free surface in a frame of reference moving with the interface. Since there are no restrictions on the horizontal components of velocity at the free surface, these turbulent components do not vary appreciably through the blockage layer. The blockage effect has been described theoretically with the source theory of Hunt and Graham [20], which treats the turbulent field as a superposition of homogeneous turbulence and an irrotational velocity field driven by a source distribution at the interface that causes the vertical velocity fluctuations to vanish there. Numerical simulations confirm this behavior (e.g., [33,35]), as do experimental observations like those of Brumley and Jirka [4] and the present work. For example, Fig. 2 shows the slight amplification of the horizontal velocity fluctuations at the expense of the vertical, the latter beginning to fall off at a depth near $\ell = 2L_{HT}$ as predicted.

The viscous effect is realized much closer to the interface. This effect is an adjustment by the flow to the condition of effectively zero tangential stress at the free surface, i.e., $\partial u/\partial z = \partial v/\partial z = 0$ on $z = 0$. These condi-

tions imply strong suppression of horizontal vorticity, while the vertical vorticity is not modified significantly. Therefore, the free-surface vortical motions at a clean interface are often dominated by normally connected vortices (see Fig. 7c). The stress-free dynamic boundary condition results in a viscous sublayer of thickness $\mathcal{O}(\ell Re_0^{-1/2})$, where $Re_0$ is based on the turbulent scales, $u_0$ and $\ell$ [5,19,33]. Over this viscous sublayer thickness, there is typically a small reduction in the horizontal velocity of an approaching eddy of $\mathcal{O}(u_0 Re_0^{-1/2})$ [19]. A similar modification occurs for the attenuation of the eddy vertical velocity, which is written as being proportional to the depth, $w \approx -(\partial u/\partial x + \partial v/\partial y)z$, in the manner shown in Section 1; the increase in the attenuation rate, relative to the inviscid case, is $\mathcal{O}(Re_0^{-1/2})$ [35]. For $Re_0 \gg 1$, these reductions are extremely small, and the viscous sublayer is of second order and negligible [5]. Thus, in the subsurface region, a clean free surface weakly damps the vertical turbulent motions while effecting minimal change to the horizontal turbulent motions. The latter allows for surface divergences and vertical fluctuations in the immediate vicinity of the interface, i.e., within the diffusive sublayer. For a scalar flux out of the water, upward velocity fluctuations bring enriched fluid toward the surface, and downward fluctuations bring depleted fluid back to the bulk. This renewal of the diffusive sublayer enhances the flux at the edges of this layer through the turbulent eddy flux [7]. Well within this layer, where the turbulent eddy flux gives way to diffusive flux, renewal events keep the concentration elevated close to the surface and the vertical gradient large, resulting in flux enhancement. The thickness of the diffusive sublayer, which is important for the gas flux, can be related to the thickness of the viscous sublayer through Schmidt number scaling, $\delta_s = \delta_m Sc^{-1/2}$, where $\delta_s$ is the gas sublayer thickness and $\delta_m$ is the viscous sublayer thickness [10]. From above, the diffusive sublayer is then $\delta_s \sim \ell Sc^{-1/2} Re_0^{-1/2}$.

For a surfactant surface, it is useful to consider the limiting case of a surface film that renders the interface completely immobile. The kinematic boundary condition at the interface for this situation is like that at a rigid wall where $u = v = w = 0$ on $z = 0$. As with the clean case, the $w = 0$ condition results in a blockage layer, while the condition $u = v = 0$ is manifest within a thinner viscous sublayer. The divergence at the interface is also zero, implying a reduction in the vertical fluctuations in the immediate vicinity of the interface. Instead of being proportional to $z$, the vertical velocity fluctuations are proportional to $z^2$ (viz., $w \sim z^2 u_0/(\ell^2 Re_0^{-1/2})$ [19], thus attenuating more rapidly when nearing a surfactant surface than when nearing a clean surface. The dynamic boundary condition at the interface is also modified, from a stress-free surface to a surface that can support a tangential stress. Again, this boundary condition influences the flow very near the surface within a viscous sublayer of thickness $\mathcal{O}(\ell Re_0^{-1/2})$ as in the clean case [19]. However, it would be more appropriate to use a velocity scale other than $u_0$ in calculating $Re_0^{-1/2}$, since a bulk velocity scale (e.g., for $z > \ell$) may be largely unaffected by surfactant effects. Because a significant difference between the clean and immobile cases is the reduction of the horizontal velocity fluctuations across the viscous sublayer, using a surface velocity scale, for example, would be more relevant. If the surface becomes fully immobilized, the horizontal velocity near the surface can be expressed as $u \sim z u_0/(\ell Re_0^{-1/2})$ [19], and the reduction is $\mathcal{O}(u_0)$. For interfaces that are still mobile, the present measurements indicate a maximum reduction in the surface velocity of about a factor of two; the simulation results of Tsai [35] indicate peak reductions between a factor of about two to six. Based on these values, the viscous sublayer, and the diffusive sublayer, then increase to thicknesses roughly 1.5–2.5 times the thicknesses found for a clean surface. A thicker diffusive sublayer implies a reduction in $k$ via the thin-film model ($k = D/\delta_s$). The above increases in the thickness of $\delta_s$ correlate to $k_{film}/k_{clean}$ of 40–67% based on the thin-film model; the actual measured ratios of $k_{film}/k_{clean}$ were closer to 30%.

When the surface becomes immobile, associated with the dramatic reduction in the horizontal turbulent eddy velocities is a viscous shear stress of $\mathcal{O}(\rho u_0^2 Re_0^{-1/2})$. This gives rise to strong horizontal vorticity production within the viscous sublayer. This feature has been shown by the simulations of Tsai [35]. Thus, the near-surface region, characterized by strong vertical gradients in the horizontal velocities, is subject to strong viscous dissipation. This highly dissipative sublayer flow damps the turbulent eddy energetics, acting like a sink layer. This can be seen as attenuating the local hydrodynamic contribution to the gas-transfer velocity parameterization through a reduction in the local $Re_0$. More importantly, the immobilized surface switches the Schmidt number power dependence from 1/2 to 2/3 [25], which will have an important effect for $Sc \gg 1$. For $O_2$, this transition means a reduction in $k$ by a factor of almost three, which is in near-quantitative agreement with the reductions observed in the present measurements. The present results indicate a factor of 3–3.5, the difference being possibly made up by the reduced local $Re_0$.

One may speculate to what degree a realistic surfactant surface, which will permit some lateral interfacial mobility, resembles a rigid wall. These experiments and the simulations of Tsai [35] have shown that the free-surface horizontal velocities, while not vanishing, can be reduced to 1/6–1/2 their clean surface values. Although the rigid wall condition ($u = v = 0$) is not strictly met, turbulence is significantly reduced at a surfactant-adsorbed free surface and the resemblance to a rigid wall emerges. Perhaps more critical is the stress boundary condition at the surface. This condition, in its most

fundamental form, expresses the balance between the fluid viscous stress and the surface Marangoni stress:

$$\mu\frac{\partial u}{\partial z}=\frac{\partial\sigma}{\partial x}. \tag{6}$$

Therefore, the ratio of the Marangoni stress to a "virtual" viscous stress due to a rigid wall provides the degree to which the surface behaves like an immobile boundary in the sense of the dynamic boundary condition. This ratio is defined as

$$\mathscr{J}=\frac{\frac{\partial\sigma}{\partial x}}{\mu\frac{\partial u}{\partial z}\big|_{\text{wall}}}. \tag{7}$$

When $\mathscr{J}=0$, the surface behaves as a clean interface; when $\mathscr{J}=1$, the surface resembles a rigid wall. It was noted above that the viscous stress due to an immobile boundary is $\mathscr{O}(\rho u_0^2 Re_0^{-1/2})$. A possible first approximation to the Marangoni stress is $\partial\sigma/\partial x\sim\pi/\ell$, giving the ratio

$$\mathscr{J}=\frac{\pi Re_0^{1/2}}{\rho u_0^2\ell}, \tag{8}$$

which can be written in terms of a Weber number and a Reynolds number,

$$\mathscr{J}=\frac{Re_0^{1/2}}{We_\pi}, \tag{9}$$

where the Weber number is defined as $We_\pi=\rho u_0^2\ell/\pi$ and is a measure of the ratio between inertial and surface pressure forces. The choice of $\ell$ as the lengthscale over which the surface tension varies by $\pi$ may be a conservative estimate; the surface tension may actually vary by such an amount over much smaller scales making $\partial\sigma/\partial x$ larger. For the conditions studied in this investigation, Eq. (9) indicates that surface pressures of 0.1 mN/m (for $Re_0=282$) to 0.6 mN/m (for $Re_0=974$) force $\mathscr{J}$ to be equal to one. This indicates that very little surface tension gradient is required to generate an interfacial stress that is comparable to the stress at a rigid wall, at least in an instantaneous sense. This result is consistent with the observed sensitivity of the flow, and $k$, to small $\pi$. Thus, in terms of surface pressure, a surfactant surface can quickly resemble a rigid wall, reducing the gas transfer notably for small values of $\pi$ toward a final limiting value.

### 3.6. Relationship between surface divergence and gas transfer

Simple scaling of the convection–diffusion equation using a stagnation flow model as in Csanady [8] yields an expression for the dimensionless gas-transfer velocity in terms of the Schmidt and Reynolds numbers:

$$k^+=\frac{k}{aL}=\mathscr{C}\,Re_a^{-1/2}\,Sc^{-n}, \tag{10}$$

where $Re_a=aL^2/\nu$ and the Schmidt number exponent $n$ is governed by the surface condition. This relationship was explored using the present gas-transfer and hydrodynamic data. In order to determine the constant $\mathscr{C}$ and the Schmidt number dependence $n$, the transfer velocity and the surface divergence data were incorporated in a least-squares regression using the model of Eq. (10). In this case, $L$ was taken to be $2L_{\text{HT}}$, evaluated at the free surface. In order to characterize $n$ in terms of a measured property of the surface, the stress ratio $\mathscr{J}$ derived in the previous section was used. A more relevant, but unavailable, quantity might involve the surface (visco)-elasticity, which is more appropriate in describing the response of the surface to in-plane straining motions. Since the observed effect of the presence of a surface film resembled an inverse power-law, or exponential, type reduction in the quantities of interest (e.g., Fig. 8), an empirical expression relating $n$ and $\mathscr{J}$ that describes the physical behavior was sought. For simplicity, the following relationship between surface pressure and $n$ was postulated:

$$n=2/3-1/6\mathrm{e}^{-\lambda\mathscr{J}}. \tag{11}$$

In this way, when $\mathscr{J}=0$, $n=1/2$, and the surface is clean; when $\lambda\mathscr{J}>1$, $n\approx 2/3$ and the surface behaves like a rigid wall. The results from the regression provided the two constants $\lambda$ and $\mathscr{C}$, yielding a relationship between surface divergence and gas transfer, written as

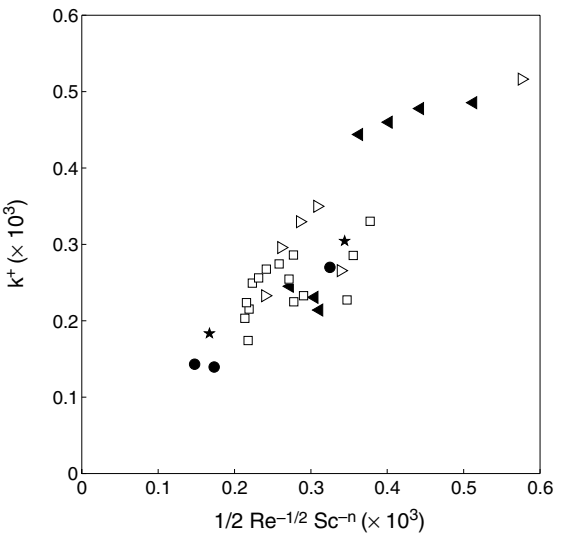


Fig. 9. Dimensionless relationship between surface divergence and gas-transfer velocity for all grid turbulence datasets using Eq. (12). All markers are as in previous figures. The axis values have been scaled by $10^3$ for clarity. $R^2=0.88$.

$$k^+ = \frac{1}{2} Re_a^{-1/2} Sc^{-n}, \quad n = 2/3 - 1/6e^{-\mathscr{S}/2}. \tag{12}$$

Plotting the $k$–$a$ data using this expression with the estimates of surface pressure as given in Table 2 yields the result shown in Fig. 9. The relationship appears reasonably robust, with only a few data points deviating noticeably. The $R^2$ statistic for this relationship was 0.88, the highest value thus far. This result is believed to be the first experimental relationship between surface divergence and gas-transfer velocity.

## 4. Conclusion

Based on coincident laboratory measurements of gas-transfer and free-surface hydrodynamics for various interfacial conditions, the surface divergence appears to be a critical process in air–water gas exchange. As expected, bulk turbulence estimates were unable to provide a unique relationship for the measured gas-transfer velocities. Free-surface turbulence was found to yield an improved relationship, however, there is evidence that such a relationship is dependent upon the nature of the flow. The surface divergence was discovered to provide a relationship for the gas transfer that accounted for the presence of surface films and did not depend on the flow types considered. The relationship obtained was derived from basic scaling of the convection–diffusion equation, and is novel in that it specifies the Schmidt number exponent using a dimensionless surface stress ratio. This ratio provides a measure of the degree to which the surface behaves as a rigid boundary. In addition, this relationship is believed to be the first experimental relationship between surface divergence and gas-transfer velocity. The success of the surface divergence model for interfacial gas transfer is thought to stem from the fact that surface divergence provides a direct measure of the surface renewal that is vital to gas-transfer enhancement. This relationship illustrates the potentially universal role of surface divergence in air–water gas exchange. It is also an attempt to relate, in a physically meaningful way, the interactions between surface renewal, surfactants, and gas transfer.

While the results herein have clearly shown the importance of surface divergence for air–water gas transfer, much research in this area has thus far failed to adequately consider surface divergence. There has been considerable effort aimed at relating transfer rates to many other physical quantities (e.g., windspeed: [3,14]; friction velocity: [14,28]; waterside velocities: [1,6,12,23,24]; wave slope: [2,21]), however, none of these studies directly address the role of surface divergence in air–water gas transport. This is reflected in recent parameterizations of air–sea gas transfer, which relate the transfer velocity to wind speed (e.g., [37]). To be sure, while measurement of wind speed over the ocean is much more feasible compared to a direct measure of the surface divergence, it is critical to maintain a focus on the underlying aspects of the problem. The results from this study are hoped to aid in that endeavor by illustrating the direct link between surface divergence and air–water gas exchange.

The free-surface flow measurements in this study were made possible by new advances in PIV. Likewise, recent advances in infrared (IR) imaging technology have enabled a novel approach to the gas-transfer measurement problem. This approach, which uses heat as a proxy tracer for mass, has been pioneered by Haussecker et al. [17] and Jessup et al. [22] with passive IR surface imaging techniques and the controlled flux technique (CFT). In the former approach, IR imagery of the water surface is used to reveal localized areas of surface renewal via disruption of the interface by microscale breaking events. Good correlations have been found between the fractional area affected by this surface renewal and the gas-transfer velocity with and without surface films. Given that microscale wave breaking involves renewal of the surface, there is a strong connection between the present study and those that look at microscale wave breaking. This is also additional evidence of the role of surface divergence in air–water gas transfer. The CFT probes gas transfer by observing the response of the water surface temperature, and its spatial variability, due to an imposed heat flux from a laser source. An attractive feature of the CFT approach is the significant improvement in the temporal resolution of gas flux measurements it provides – time scales for this type of measurement are on the order of seconds as compared to minutes or hours.

Finally, although this study is fundamental in nature and limited to the laboratory, implications for real systems exist. Given the type of turbulence studied, there is a potential connection to riverine systems and oceanographic systems where there is a subsurface source of turbulence. It is also possible that the surface divergence results from this study may have a much wider range of applicability since there is evidence that surface divergence is a fundamental process driving air–water transport. If this is indeed the case, then regardless of the dynamic forcing responsible for generating mixing at an air–water interface (e.g., wind, waves, bottom turbulence, natural convection, etc.), surface divergences will be generated and the intensity of these divergences will be directly linked to the transport. This behavior was observed in the present experiments with the consideration of the waves dataset. By exploring a fundamental aspect of the transport process, these results may prove to be of a general nature and therefore transferable to a wide variety of systems. One area that further studies may be able to probe is the influence of the temporal and

spatial scales of the surface divergence on air–water transport.

## Acknowledgements

This work was supported by the Woods Hole Oceanographic Institution Ocean Ventures Fund and the Andrew W. Mellon Foundation for Innovative Research. This is Woods Hole Oceanographic Institution Contribution 11003.

## References

[1] W.E. Asher, J.F. Pankow, The interaction of mechanically generated turbulence and interfacial films with a liquid phase controlled gas/liquid transport process, Tellus 38 (1986) 305–318.
[2] E.J. Bock, T. Hara, N.M. Frew, W.R. McGillis, Relationship between air–sea gas transfer and short wind waves, J. Geophys. Res. 104 (C11) (1999) 25821–25831.
[3] H.-C. Broeker, J. Petermann, W. Siems, The influence of wind on $CO_2$-exchange in a wind-wave tunnel, including the effects of monlayers, J. Mar. Res. 36 (1978) 595–610.
[4] B.H. Brumley, G.H. Jirka, Near-surface turbulence in a grid-stirred tank, J. Fluid Mech. 183 (1987) 235–263.
[5] B.H. Brumley, G.H. Jirka, Air–water transfer of slightly soluble gases: turbulence, interfacial processes and conceptual models, PhysicoChem. Hydrodyn. 10 (1988) 295–319.
[6] C.R. Chu, G.H. Jirka, Turbulent gas flux measurements below the air–water interface of a grid-stirred tank, Int. J. Heat Mass Transfer 35 (1992) 1957–1968.
[7] M. Coantic, A model of gas transfer across air/water interfaces with capillary waves, J. Geophys. Res. 91 (1986) 3925–3943.
[8] G.T. Csanady, The role of breaking wavelets in air–sea gas transfer, J. Geophys. Res. 95 (1990) 749–759.
[9] J.T. Davies, The effects of surface films in damping eddies at a free surface of a turbulent liquid, Proc. Roy. Soc. Lond. A 290 (1966) 515–526.
[10] J.T. Davies, E.K. Rideal, Interfacial Phenomena, Academic Press, New York, NY, 1963.
[11] I.P.D. De Silva, H.J.S. Fernando, Oscillating grids as a source of nearly isotropic turbulence, Phys. Fluids 6 (1994) 2455–2464.
[12] T.D. Dickey, B. Hartman, D. Hammond, E. Hurst, A laboratory technique for investigating the relationship between gas transfer and fluid turbulence, in: W. Brutsaert, G.H. Jirka (Eds.), Gas Transfer at Water Surfaces, D. Reidel Publishing Company, Minneapolis, MN, 1984, pp. 93–100.
[13] J. George, F. Minel, M. Grisenti, Physical and hydrodynamic parameters controlling gas–liquid mass transfer, Int. J. Heat Mass Transfer 37 (1994) 1569–1578.
[14] N.M. Frew, E.J. Bock, W.R. McGillis, A.V. Karachintsev, T. Hara, T. Münsterer, B. Jähne, Variation of air–water gas transfer velocity with wind stress and surface viscoelasticity, in: B. Jähne, E. Monahan (Eds.), Air–Water Gas Transfer, AEON Verlag, Heidelberg, Germany, 1995, pp. 529–541.
[15] J.C. Goldman, M.R. Dennet, N.M. Frew, Surfactant effects on air–sea gas exchange under turbulent conditions, Deep Sea Res. 35 (1988) 1953–1970.
[16] J.S. Gulliver, A. Tamburrino, Turbulent surface deformation and their relationship to mass transfer in an open-channel flow, in: B. Jähne, E. Monahan (Eds.), Air–Water Gas Transfer, AEON Verlag, Heidelberg, Germany, 1995, pp. 589–600.
[17] H. Haussecker, S. Reinelt, B. Jähne, Heat as a proxy tracer for gas exchange measurements in the field: principles and technical realization, in: B. Jähne, E. Monahan (Eds.), Air–Water Gas Transfer, AEON Verlag, Heidelberg, Germany, 1995, pp. 405–413.
[18] E.J. Hopfinger, J.-A. Toly, Spatially decaying turbulence and its relation to mixing across density interfaces, J. Fluid Mech. 78 (1976) 155–175.
[19] J.C.R. Hunt, Turbulence structure and turbulent diffusion near gas–liquid interfaces, in: W. Brutsaert, G.H. Jirka (Eds.), Gas Transfer at Water Surfaces, D. Reidel Publishing Company, Minneapolis, MN, 1984, pp. 67–82.
[20] J.C.R. Hunt, J.M.R. Graham, Free-stream turbulence near plane boundaries, J. Fluid Mech. 84 (1978) 209–235.
[21] B. Jähne, K.O. Münnich, R. Bösinger, A. Dutzi, W. Huber, P. Libner, On the parameters influencing air–water gas exchange, J. Geophys. Res. 92 (1987) 1937–1949.
[22] A.T. Jessup, C.J. Zappa, V. Hesany, M.R. Loewen, M.G. Skafel, Dependence of the skin layer recovery rate on heat flux and turbulence, in: B. Jähne, E. Monahan (Eds.), Air–Water Gas Transfer, AEON Verlag, Heidelberg, Germany, 1995, pp. 601–610.
[23] B.-C. Khoo, A.A. Sonin, Scalar rate correlation at a turbulent liquid free surface: a two-regime correlation for high Schmidt numbers, Int. J. Heat Mass Transfer 35 (1992) 2233–2244.
[24] S. Komori, R. Nagaosa, Y. Murakami, Turbulence structure and mass transfer across a sheared air–water interface in wind-driven turbulence, J. Fluid Mech. 249 (1993) 161–183.
[25] J.R. Ledwell, Variation of the gas transfer coefficient with molecular diffusivity, in: W. Brutsaert, G.H. Jirka (Eds.), Gas Transfer at Water Surfaces, D. Reidel Publishing Company, Minneapolis, MN, 1984, pp. 293–302.
[26] P.S. Liss, P.G. Slater, Flux of gases across the air–sea interface, Nature 247 (1973) 181–184.
[27] M.J. McCready, E. Vassiliadou, T.J. Hanratty, Computer simulation of turbulent mass transfer at a mobile interface, Am. Inst. Chem. Engrs. 32 (1986) 1108–1115.
[28] W.R. McGillis, J.W.H. Dacey, N.M. Frew, E.J. Bock, R.K. Nelson, Water–air flux of dimethylsulfide, J. Geophys. Res. 105 (2000) 1187–1193.
[29] S.P. McKenna, Free-surface turbulence and air–water gas exchange, Ph.D. Thesis, Massachusetts Institute of Technology, Cambridge, MA, 2000.
[30] J.R. Saylor, G.B. Smith, K.A. Flack, The effect of a surfactant monolayer on the temperature field of a water surface undergoing evaporation, Int. J. Heat Mass Transfer 43 (2000) 3073–3086.
[31] L.E. Scriven, Dynamics of a fluid interface, Chem. Eng. Sci. 12 (1960) 98–108.

[32] L. Shen, G.S. Triantafyllou, D.K.P. Yue, Turbulent diffusion near a free surface, J. Fluid Mech. 407 (2000) 145–166.
[33] L. Shen, X. Zhang, D.K.P. Yue, G.S. Triantafyllou, The surface layer for free-surface turbulent flows, J. Fluid Mech. 386 (1999) 167–212.
[34] S.M. Thompson, J.S. Turner, Mixing across an interface due to turbulence generated by an oscillating grid, J. Fluid Mech. 67 (1975) 349–368.
[35] W.T. Tsai, Impact of a surfactant on a turbulent shear layer under the air–sea interface, J. Geophys. Res. 101 (1996) 28557–28568.
[36] W.T. Tsai, D.K.P. Yue, Effects of soluble and insoluble surfactant on laminar interactions of vortical flows with a free surface, J. Fluid Mech. 289 (1995) 315–349.
[37] R. Wanninkohf, W.R. McGillis, A cubic relationship between air–sea $CO_2$ exchange and wind speed, Geophys. Res. Lett. 26 (1999) 1889–1892.